VII International Conference on Particle-Based Methods
PARTICLES 2021
P. Wriggers, M. Bischoff, E. Oñate, M. Bischoff, A. Düster & T. Zohdi (Eds)

OPTIMIZING THE SHAPE OF PLANETARY ROVER WHEELS USING DEM AND BAYESIAN OPTIMIZATION

LEON STUBBIG AND ROY LICHTENHELDT

Institute of System Dynamics and Control
German Aerospace Center (DLR)
Münchener Straße 20, 82234 Weßling, Germany
[leon.stubbig, roy.lichtenheldt]@dlr.de, www.dlr.de/sr

Key words: DEM, Planetary Exploration, Low Gravity, Rover Wheels, Optimization

Abstract. The Martian Moons eXploration mission will include a rover to conduct in situ science and exploration on the Martian moon Phobos. The rover's locomotion system and especially its wheels require special consideration, as wheeled locomotion has never been employed in a comparably low gravity environment. This paper shows an automated approach to design the shape of rover wheels using high-fidelity simulation models based on the Discrete Element Method and a Bayesian Optimization algorithm. Four main parameters were selected to describe the wheel shape: grouser height, grouser number, grouser chevron angle and rim curvature. On Phobos, three main scenarios are important to ensure the rover's successful operation: Driving forward, backward, and up slopes. The optimization loop thus generates wheels within given limits for the four wheel shape parameters, runs a simulation of a single wheel experiment with free slip conditions for each scenario, and assesses the wheel's performance based on the distance travelled. The found wheel shape performs 64 % better than the previous prototype and, in combination with the found parameter relations, will guide the design of the wheels for the MMX mission.

1 INTRODUCTION

The Martian Moons eXploration (MMX) mission is lead by the Japanese Aerospace Exploration Agency (JAXA) and will explore the moons of Mars: Phobos and Deimos. The mission's focus is research of the moons' origin and the return of samples from the surface of the larger of the two moons: Phobos. The main spacecraft is going to be accompanied by a small, four-wheeled rover that is going to land on Phobos prior to the spacecraft [1]. This rover is currently under development at the French and German space agencies, the Centre national d'études spatiales (CNES) and German Aerospace Center (DLR). The rover will perform in-situ exploration of the surface of Phobos and assist with the sample site selection and hazard avoidance for the spacecraft.

The MMX Rover will operate in lower gravity than any other wheeled rover before, providing unique challenges to its locomotion system [2]. In particular, the interaction

of the rover's wheels with the regolith on Phobos is difficult to predict as the mechanics of granular materials have been shown to be gravity dependent [3, 4] and wheel-soil interaction dynamics are slow, which limits the amount of testing that can be done in low-gravity facilities on Earth. Additionally, the surfaces of small bodies in the solar system have been shown to vary widely and little is known about the characteristics of Phobos' surface at the scale relevant to the rover. Wheel design for the MMX Rover is therefore based on a broad modeling and simulation study.

This paper is structured as follows. First, background on wheel design for planetary rovers and important design considerations are given. Then, the Discrete Element Method (DEM) and the simulation model are explained, and the optimization strategy is presented. Finally, results specific to the MMX Rover as well as general insights about wheel parameter dependence are shown and conclusions are drawn.

2 CHALLENGES, WHEEL DESIGN AND PREPARATIONS

Rocky solar system bodies pose severe challenges to the design of rovers and their locomotion system: For example, the movement of NASA's Mars rovers has been hindered by patches of soft soil where wheels sink in deep and are in danger of permanent entrapment [5]. Large rocks and boulders can be another obstacle. For example, when JAXA's Hayabusa 2 probe reached 162173 Ryugu, it was found that the asteroid has a much rockier surface than expected. Phobos itself has not been visited by any surface probes. Remote sensing data available from multiple Mars missions shows a surface with impact craters of various sizes but otherwise smooth terrain down to a resolution of about 1.5 m per pixel [6], which is the highest resolution available for a few selected areas. Figure 1 shows a global view of Phobos at a coarser resolution.

This high uncertainty on the terrain on Phobos means that reasonable assumptions had to be made for the MMX mission [6]. The rover needs a robust locomotion system that is able to deal with a variety of terrains, ranging from soft, powdery soil to hard, rocky surfaces. From this range, the rover team has identified very soft soil as the greater danger. While permanent immobilization is unlikely on hard terrain, high wheel sinkage in soft soil can permanently trap a rover and end it's mobile mission, as happened to the Spirit rover on Mars [5].

Another cause of uncertainty is the limited understanding of granular mechanics in low gravity. Granular materials have been shown to exhibit gravity dependent properties that are not fully understood yet [3, 4, 8].

Wheels for planetary rovers have a few common characteristics: They are relatively large in order to reduce soil pressure below the wheels and thus sinkage. They are also equipped with grousers. These features on the wheel rim have been shown to tremendously improve the traction capabilities of rigid wheels on loose granular materials [9] and have been employed in most rover wheel designs to date. The dimensioning of grousers depends on the operation environment and requires dedicated studies for each new wheel design. Previous studies to design grousers were often driven by experiments on Earth [10, 11], geometrical considerations [12], and increasingly often by simulation [13, 14, 15].

Early rover testing for MMX has been performed with the prototype wheel shown in

Figure 2. Its design is based on previous simulation results for a small Mars rover [16] and engineering considerations. The grousers of the prototype wheel have a "shovel shape". These shapes as well as grouser number, grouser height and chevron angle were investigated in a previous "One-Factor-at-a-Time" optimization study [15] which concluded that the shovel radius is unlikely to have a considerable effect in low gravity environments. The wheel resulting from the effort in [15] is shown in Figure 3. Both wheels serve as a reference and point of comparison for the study at hand.

Figure 1: Phobos at a resolution of 5.8 m per pixel [NASA/JPL/University of Arizona][7]

Figure 2: The prototype for the MMX wheel [2]

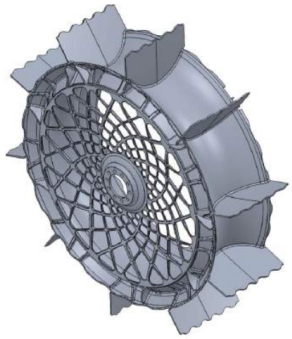

Figure 3: The resulting wheel from a previous optimization effort [15]

3 SIMULATION MODEL

The chosen method to simulate the interaction of rover wheels with soft soil is DEM [17]. In this section the method, the chosen parameters and the employed approach for conducting single wheel experiments are explained.

3.1 The Discrete Element Method

In DEM, the regolith is discretized into spherical particles that interact based on contact laws. Specifically, a HERTZian contact model is used with linear damping in the normal direction to compute the normal force $\vec{F}_\mathrm{n}$ acting between two contacting particles i and j [18]:

$$\vec{F}_\mathrm{n}^{ij} = \left(\frac{2E}{3\left(1-\nu^2\right)} \sqrt{r_c^{ij} \left|\vec{\delta}_n^{ij}\right|} \right) \vec{n}^{ij} + k^{ij} \dot{\vec{\delta}}_n^{ij}, \tag{1}$$

where E is YOUNG's modulus, ν is POISSON ratio, r_c^{ij} is the contact radius, i.e. the average of the contacting spheres' radii r_i and r_j, δ_n^{ij} is the normal overlap and k^{ij} is the damping coefficient. The latter is computed as a fraction D of the critical damping coefficient k_crit^{ij} [18]:

$$k^{ij} = D k_\mathrm{crit}^{ij} = \frac{4}{3} D \sqrt{\frac{2\rho E \pi \left(r_\mathrm{min}^{ij}\right)^4}{1-\nu}} \sqrt{|u|}, \tag{2}$$

where u is an allowed maximum overlap of 0.25 and ρ is density.

In the tangential direction stick-slip friction is modeled based on COULOMB friction with a KELVIN element for regularization [18]:

$$\vec{F}_{\mathrm{cT}}^{ij} = c_{\mathrm{T}}\vec{\delta}_{\mathrm{T}}^{ij}\mathrm{sign}\left(\vec{\delta}_{\mathrm{T}}^{ij}\dot{\vec{\delta}}_{\mathrm{T}}^{ij}\right) + k_{\mathrm{T}}\dot{\vec{\delta}}_{\mathrm{T}}^{ij} \tag{3}$$

$$\vec{F}_{\mathrm{T}}^{ij} = \begin{cases} \vec{F}_{\mathrm{cT}}^{ij} & \forall|\vec{F}_{\mathrm{cT}}^{ij}| \leq |\vec{F}_{\mathrm{n}}^{ij}|\tan\left(\phi_{\mathrm{h}}\right) \wedge |\dot{\vec{\delta}}_{\mathrm{T}}^{ij}| \leq v_{\mathrm{Tmin}} \\ \vec{F}_{\mathrm{n}}^{ij}\tan\left(\phi_{\mathrm{g}}\right)\left(\dot{\vec{\delta}}_{\mathrm{T}}^{ij}\right)_0 & \forall|\vec{F}_{\mathrm{cT}}^{ij}| > |\vec{F}_{\mathrm{n}}^{ij}|\tan\left(\phi_{\mathrm{h}}\right) \vee |\dot{\vec{\delta}}_{\mathrm{T}}^{ij}| > v_{\mathrm{Tmin}} \end{cases}, \tag{4}$$

where $\vec{F}_{\mathrm{cT}}^{ij}$ is the force of the KELVIN element, which is computed from the tangential stiffness c_T, displacement δ_{T} and damping coefficient k_{T}. If the KELVIN force is smaller than the sticking force computed using the sticking friction angle ϕ_{h} and if the tangential velocity $\dot{\vec{\delta}}_{\mathrm{T}}^{ij}$ is lower than the stick velocity limit v_{Tmin}^{ij}, the KELVIN force is used. Otherwise, a tangential slipping force computed using the slipping friction angle ϕ_{g} is applied.

The rotational behavior of real soil particles depends on their potentially irregular shape. For computational reasons (e.g. contact detection) most DEM codes employ spherical particles. In order to improve rotations a rolling resistance model [19] was implemented and is used with a relatively high rolling resistance coefficient of 0.99.

Equating all acting forces and torques and integrating the equations of motion based on NEWTON's and EULER's equations then yields positions and rotations of all particles over time. A specialized implicit integrator provides a good balance between speed and accuracy [20]. Rigid bodies can be imported as a mesh and interact in a similar fashion.

The DEM simulation model is implemented in "partsival", a tool developed at DLR that enables fast simulations using a computer's Graphics Processing Unit (GPU) [21]. It has previously been used for various studies concerning wheels and planetary soils, e.g. [22, 23]. A recent validation study specific to rover wheels was carried out in [24].

3.2 Simulation parameters

Regolith parameters were derived from [6] to create a challenging soft soil. The particle radii range is set to 2.4 mm to 3 mm. The maximum radius is hereby estimated based on the "tool resolution" [18]:

$$\Gamma := \frac{L_{\mathrm{min}}}{2r_{\mathrm{max}}}, \tag{5}$$

that relates the largest particle radius r_{max} to the length of the smallest surface feature on the interacting tool L_{min}. For rover wheels, this is the grousers height h. A tool resolution greater than 2.5 has been found to be sufficient [18]. With a radius of 3 mm, this corresponds to a grouser height of 15 mm. During the optimization the same particle size is also used for shorter grousers. This is an acceptable trade-off of accuracy at the edges of the search space for simulation speed and comparability between simulations.

The effective surface acceleration on Phobos is comprised of gravity as well as Mars tides and centrifugal acceleration. It ranges from 3.0×10^{-3} to $6.8 \times 10^{-3}\,\mathrm{m\,s^{-2}}$ [6]. In this study an effective surface gravity towards the higher end of the observed range of $6 \times 10^{-3}\,\mathrm{m\,s^{-2}}$ was chosen. This is 1/2000 of gravity on Earth.

Particle density is set to $2\,600\,\mathrm{kg\,m^{-3}}$ which is in line with sands on Earth and models for Phobos regolith. Similarly, the Poisson ratio ν is set to 0.15, which is an average value for common quartz sands. The YOUNG's modulus is derived using Equations 9 and 10 in [18], which yield a range of $4.6 \times 10^3\,\mathrm{Pa}$ to $4.8 \times 10^4\,\mathrm{Pa}$. A value of $3 \times 10^4\,\mathrm{Pa}$ was used.

Friction angles are set to 25° and 27° for particle-to-particle sliding and sticking friction, respectively. Friction between particles and container walls as well as the wheel mesh are set to similar values at 25° for sliding friction and 26° for sticking friction.

The soil is assumed to be cohesionless. This is a worst case assumption based on preparatory DEM simulations [15]. Table 1 shows an overview of the chosen parameters and simulation settings.

Table 1: Parameters and simulation settings

	Parameter	Symbol	Value
DEM	Young's modulus	E	$3 \times 10^4\,\mathrm{Pa}$
	Poisson ratio	ν	0.15
	Particle density	ρ	$2\,600\,\mathrm{kg\,m^{-3}}$
	Critical damping factor	D	0.4
	Gravitational acceleration	g	$6 \times 10^{-3}\,\mathrm{m\,s^{-2}}$
	Maximum particle velocity	$v_{\max}$	$0.5\,\mathrm{m\,s^{-1}}$
	Slip friction angle (particles)	ϕ_{slip}	25°
	Stick friction angle (particles)	ϕ_{stick}	27°
	Rolling resistance	R	0.99
	Slip friction (container and mesh)	$\phi_{\mathrm{slip_{mesh}}}$	25°
	Stick friction (container and mesh)	$\phi_{\mathrm{stick_{mesh}}}$	26°
	Particle radius	r	[2.4 mm, 3 mm]
	Cohesion	c	0 Pa
Simulation	Duration	t_{total}	50 s
	Loading	m	6.25 kg
	Container length	x	1.6 m
	Container width	y	0.16 m
	Container depth	z	0.34 m
	Wheel velocity	ω_y	$0.25\,\mathrm{rad\,s^{-1}}$
	Wheel acceleration	$\dot{\omega}_y$	$0.04\,\mathrm{rad\,s^{-2}}$
	Wheel revolutions	n_{wheel}	1.57
Solver	Floating point precision		double
	Variable step		yes
	Maximum time step size	$\Delta t_{\max}$	$1.3 \times 10^{-4}\,\mathrm{s}$
	Corrector iterations	$n_{\mathrm{corrector}}$	3

3.3 Soil preparation

Flat and sloped soil beds are prepared to be reloaded in each wheel simulation. Soil preparation is conducted by initializing a particle package a few milimeters above the

ground of the container with slightly randomized positions. The particles are then released and settle into the container under the force of gravity. Under Phobos gravity this settling takes about 30 s of simulated time. For slope simulations the gravity vector tilted by 10°.

The following considerations apply to the container size: Its cross-section needs to be large enough to avoid boundary effects. To reduce the total amount of particles and thus computation time it also has to be chosen as small as possible. The length of the container has little effect on simulation time due to the use of dynamic simulation boundaries that follow the wheel's position [22]. The container thus has a width of 16 cm, a height of 35 cm and a length of 160 cm. The prepared soil bed has a height of 17 cm.

3.4 Single wheel experiments

The rover is anticipated to weigh 25 kg [1] resulting in a mass loading of 6.25 kg per wheel. At the start of a simulation, the wheel is positioned right above the surface of a soil bed, released, and given some time to settle, before the wheel starts to rheonomically operate. A constant angular acceleration causes a ramp-like velocity profile with its maximum at 0.25 rad s^{-1} reached after 13.5 s. The wheel is constrained to the x-z plane and a total of 50 s is simulated.

The number of particles can be cut in half by exploiting the simulation's symmetry: The investigated wheels are symmetric with respect to the x-z plane, allowing for a reduction of the simulated soil domain by half as described in [22]. Another measure to save computational time is the use of dynamic boundaries [22]. They restrict the volume of active particles to a domain of 0.5x0.3x0.5m^3 around the wheel. The simulation's geometry and kinematics are shown in Figure 4.

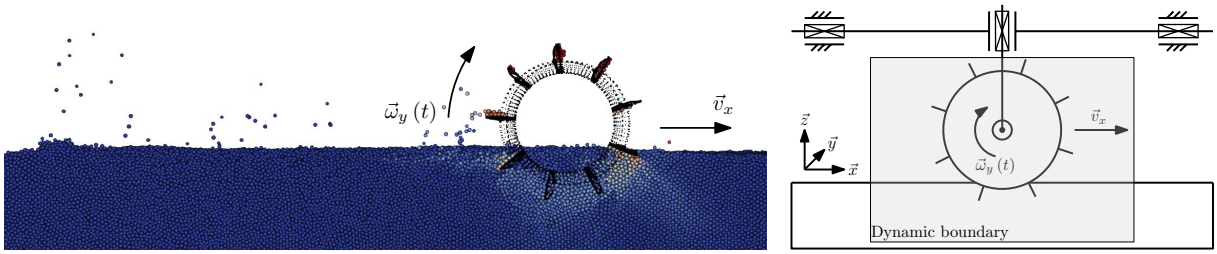

Figure 4: An exemplary wheel simulation (left) and the corresponding kinematic model (right)

To determine wheel performance in a way that is relevant to the mission, three scenarios were defined: In the first one the wheel drives forward on a flat soil bed, in the second one it drives backward and in the third one it drives straight up a 10° slope. Each of these simulations takes about 20 h in double precision on a Nvidia V100 GPU.

4 OPTIMIZATION STRATEGY

Bayesian optimization (BO) as implemented in Matlab [25] is used to perform the optimization. The algorithm was chosen based on a preliminary study where BO was compared to a range of population-based optimization algorithms (Genetic Algorithm, Particle

Swarm Optimization, Differential Evolution and an Evolutionary Strategy algorithm). It was found that BO consistently finds better optima in fewer iterations while having a good coverage of the search space. The computational overhead of BO is insignificant in this application where each fitness evaluation takes multiple hours to compute.

BO is a global optimization approach that models the fitness function as a Gaussian Process (GP) between each fitness evaluation and uses this GP as a surrogate model to optimize the location of the next fitness evaluation. As more points are evaluated, the GP model improves and is able to guide the optimizer. In other words, the expected knowledge gain from each new sample point is statistically modelled and optimized, reducing the number of iterations until convergence. This makes this algorithm well suited for "expensive" problems like the one at hand. The used acquisition function, "expected-improvement-plus", provides a good balance between exploration and exploitation [25]. The used kernel function "ARD Matern 5/2" has separate length scales for each parameter and a good fitting capability for unknown, smooth functions [25]. Other welcome characteristics of BO are the suitability for mixed-integer optimization, for continuous, black box fitness functions without derivative information and parallel fitness evaluations. Details about BO can be found in literature [26, 27].

The traveled distance x is used as the measure for wheel performance and weighted relative to the performance of the intermediate prototype design, shown in Figure 3, in each of the three scenarios (64 cm, 36 cm and 68 cm in the flat, slope, and reverse scenarios, respectively):

$$\mathit{fitness} = -\frac{1}{3}\left(\frac{x_{\text{flat}}}{64\,\text{cm}} + \frac{x_{\text{slope}}}{36\,\text{cm}} + \frac{x_{\text{reverse}}}{68\,\text{cm}}\right), \tag{6}$$

resulting in a good balance of the optimized wheel's desired properties: Driving forward and driving on a flat surface is more important during operations than driving backwards or on a slope. Both characteristics are therefore present in two scenarios. The normalization balances the covered distances and makes sure that each scenario is considered equally. A fitness of -1 thus corresponds to the intermediate prototype's performance with lower values indicating an improved performance.

Four parameters that determine the wheel shape are chosen as optimization parameters: Grouser number n, grouser height h, chevron angle α and rim curvature r. Table 2 shows the limits and the corresponding values of the prototype (PT) and intermediate design wheels. Figure 5 shows the wheel geometry and the respective parameters.

Table 2: Optimization parameters and values for the prototype and intermediate design wheels

Parameter		Lower boundary	Upper boundary	PT	Intermediate
Grouser number	n	5	25	9	9
Grouser height	h	0.5 cm	7 cm	3.3 cm	3.5 cm
Rim curvature	r	6 cm	−3 cm	−2.74 cm	−2.74 cm
Chevron angle	α	−30°	15°	15°	0°

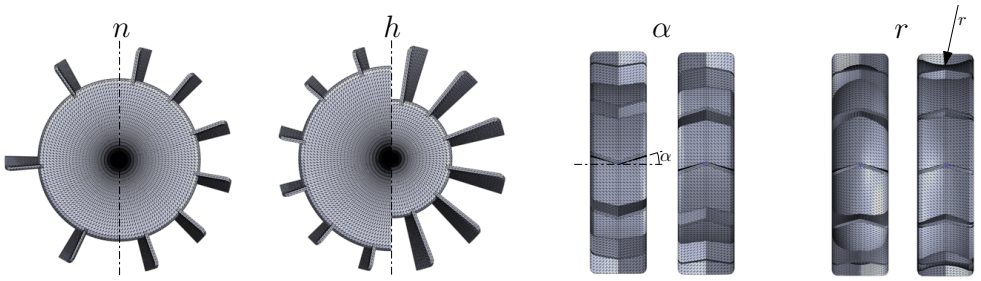

Figure 5: Wheel shape parameterization

The two most important parameters to improve wheel performance on soft soils are not included here: wheel radius and wheel width. As it is well documented that larger wheel perform better [16], these values were chosen as large as the storage space on the MMX spacecraft allows with a width of 5.3 cm and a radius of 10.4 cm. The outer wheel radius is therefore constant and an increase of the grouser height h causes an equal reduction in the rim height.

The rim curvature is given as a radius and should include flat surfaces as well as curved rims in both directions. The interval of r is therefore $r \in (-\infty, -3\text{cm}] \wedge [6\text{cm}, \infty)$, where negative radii correspond to a concave rim. A transformation function is needed to map these ranges to a continuous interval between real numbers that can be handled by the optimizer:

$$r = \frac{0.06}{r_{\text{opt}}} \qquad \text{with} \quad r_{\text{opt}} \in [-2, 1]. \tag{7}$$

5 RESULTS

The optimization was run for 115 iterations. The progress of the fitness value is shown in Figure 6. Three phases can be seen: Up to iteration 44 the evaluation points were chosen randomly to allow the optimizer to build a GP surrogate model. Between iterations 45 and 59 the model is exploited to quickly find a good minimum. After iteration 60 only small improvements to the optimum could be made and the optimizer performs more exploration. The optimization was intentionally kept running to better cover the search space and allow for the identification of broader trends. The improved search space coverage also increases the confidence that the found minimum is close to the global optimum.

5.1 The best wheel found

The wheel found is shown in Figure 7. It has 7 grousers with a length of 6.05 cm and a chevron angle of 1.2°. Its rim has a radius of curvature of −3 cm. It covered distances of 68.6 cm, 41.0 cm and 69.8 cm in the flat, slope, and reverse scenarios, respectively. Compared to the intermediate design wheel [15] this constitutes a fitness improvement of 8 %. Compared to the previous prototype wheel [2] it is an improvement of 64 %.

During the second half of the flat simulations the optimized wheel experiences an average slip of about 25 %. For comparison, the prototype wheel experienced 50 % slip in flat driving and the intermediate wheel design experienced 35 % slip in the same scenarios. Slip is increased for the slope scenario where it reaches the 60 % mark. Due to the chosen

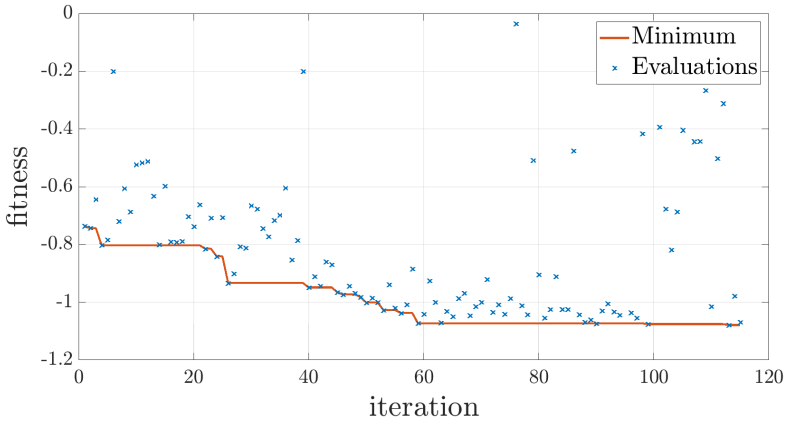

Figure 6: Progress of the optimization

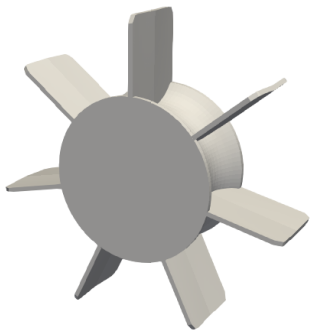

Figure 7: The best wheel found

soft soil, sinkage in the simulations is relatively high, reaching 7.5 cm in the flat and forward simulations, which is 1.5 cm below the inner rim.

5.2 Wheel shape trends

The optimization results represent a data set that allows to deduct general insights about wheel performance on the simulated soft soil in low gravity conditions. Figure 8 shows how fitness depends on each individual parameter. Next to the individual evaluations the plots also show the corresponding minimum in the final GP model, giving a clearer view of parameter dependencies. As the GP considers noisy evaluations, the resulting model does not cross each data point. The noise standard deviation estimated by the GP fit is 2.3 %, which fits the noise observed in previous DEM studies and test simulations.

It can be seen in Figure 8 that the grouser height has the most influence on the wheel's performance, i.e. the steepest parameter dependence, closely followed by the grouser number. Grousers should therefore be taller than about 4 cm and the wheel should have between 6 and 10 grousers. The third most important parameter is the chevron angle. The results show a preference towards flat grousers between about $-10°$ to $8°$. The fitness dependence on the rim curvature is less pronounced with a tendency towards inward curvatures. As the curvature of -3 cm, i.e. $r_{\text{opt}} = -2$, is close to the smallest geometrically possible value with a wheel width of 5.3 cm, the search was not extended towards even smaller radii of curvature.

As the optimization was free to chose parameter combinations in 4D space, it is also possible to investigate parameter correlations. Figure 9 shows 2D scatter plots of the computed fitness for all parameter combinations, each with the corresponding GP model minimum as a surface plot in the background. Again, it can be seen that grouser height and number have the clearest influence on wheel performance. It can also be seen in the top left plot, that these parameters are correlated. Smaller grousers work well with a larger grouser number and vice-versa. This is in line with previous research [12].

Another correlation can be seen in the grouser height – chevron angle plot in the bottom left of Figure 9. Negative chevron angles, i.e. angles that push soil towards the center of

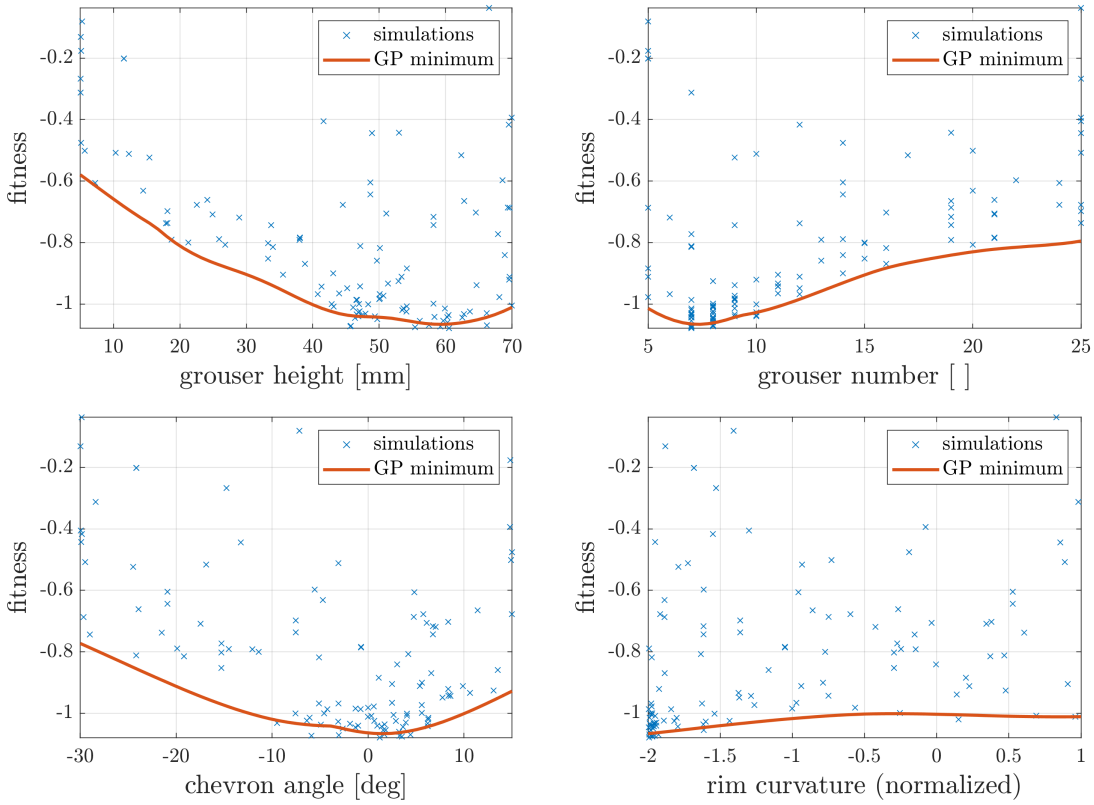

Figure 8: Individual wheel parameter dependencies

the wheel, seem to be more favorable in combination with shorter grousers. Large grousers on the other hand work better when they are flat. Previous research has found negative chevron angles to aid traction on regolith in Martian gravity, especially driving up slopes [16]. In contrast to that study, the wheels here experienced an increased sinkage which could favor grouser size over angled grousers.

6 CONCLUSION

The development of a wheel suitable for the MMX Rover and its mission on the Mars moon Phobos is a challenging endeavor due to low gravity and unknown surface properties. A simulation- and optimization-based methodology was developed and implemented to tackle this problem. A worst-case scenario consisting of soft, cohesionless soil was derived and implemented in a DEM simulation. This soil is used to conduct single wheel experiments in an optimization loop that finds suitable wheel shapes in an automated fashion. The optimized wheel performs 64 % better than the previous prototype. In combination with the simulation data and derived parameter dependencies the method yields guidelines for a new and improved wheel design for the MMX Rover and insights into wheel behavior in low gravity environments. Future work will include targeted simulations of scenarios that could not be covered during the optimization, simulations covering cohesive soils, and the mechanical design of the MMX Rover wheel's flight model.

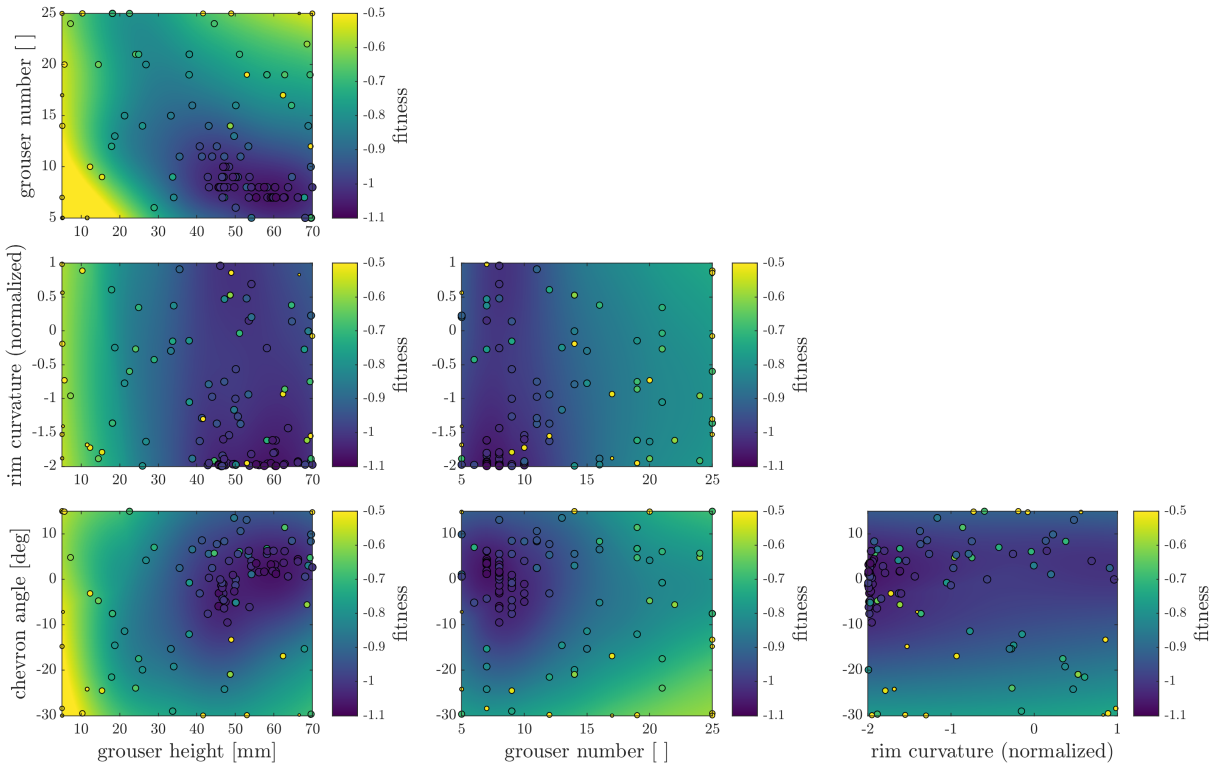

Figure 9: 2D parameter dependencies

REFERENCES

[1] S. Ulamec, P. Michel, *et al.*, "A rover for the JAXA MMX mission to Phobos," in *70th International Astronautical Congress (IAC)*, 2019.

[2] H.-J. Sedlmayr, S. Barthelmes, *et al.*, "MMX – Development of a Rover Locomotion System for Phobos," in *2020 IEEE Aerospace Conference*, pp. 1–10, IEEE, 2020.

[3] A. Brucks, T. Arndt, *et al.*, "Behavior of flowing granular materials under variable g," *Physical Review E*, vol. 75, no. 3, p. 032301, 2007.

[4] M. G. Kleinhans, H. Markies, *et al.*, "Static and dynamic angles of repose in loose granular materials under reduced gravity," *Journal of Geophysical Research: Planets*, vol. 116, no. E11, 2011.

[5] R. E. Arvidson, J. F. Bell, *et al.*, "Spirit Mars Rover Mission: Overview and selected results from the northern home plate winter haven to the side of scamander crater," *Journal of Geophysical Research: Planets*, vol. 115, no. E7, 2010.

[6] S. Tardivel and J. Biele, "Phobos environment requirement document for the MMX rover mission," tech. rep., CNES & DLR, 2019.

[7] N. Bridges, "Phobos imaged by HiRISE." `https://www.uahirise.org/phobos.php`, 2008. Accessed: 2021-04-25.

[8] C. Atwood-Stone and A. S. McEwen, "Avalanche slope angles in low-gravity environments from active martian sand dunes," *Geophysical Research Letters*, vol. 40, pp. 2929–2934, 2013.

[9] A. A. F. Nassiraei and K. Skonieczny, "Grousers improve drawbar pull by reducing resistance and generating thrust at the front of a wheel," *Journal of Terramechanics*, vol. 91, pp. 73–84, 2020.

[10] M. Sutoh, K. Nagaoka, *et al.*, "Design of wheels with grousers for planetary rovers traveling over loose soil," *Journal of Terramechanics*, vol. 50, no. 5-6, pp. 345–353, 2013.

[11] K. Nagaoka, K. Sawada, and K. Yoshida, "Shape effects of wheel grousers on traction performance on sandy terrain," *Journal of Terramechanics*, vol. 90, pp. 23–30, 2020.

[12] K. Skonieczny, S. J. Moreland, and D. S. Wettergreen, "A grouser spacing equation for determining appropriate geometry of planetary rover wheels," in *IEEE/RSJ International Conference on Intelligent Robots and Systems*, pp. 5065–5070, 2012.

[13] R. Briend, "Modelling wheel-soil interactions using the discrete element method for tread shape optimization," Master's thesis, McGill University Library, 2010.

[14] H. Nakashima, T. Yoshida, *et al.*, "Comparison of gross tractive effort of a single grouser in two-dimensional DEM and experiment," *Journal of Terramechanics*, vol. 62, pp. 41–50, 2015.

[15] F. Buchele and R. Lichtenheldt, "Multi-parameter rover wheel and grouser optimization for deployment in phobos mili-g environment," in *International Symposium on Artificial Intelligence, Robotics and Automation in Space*, 2020.

[16] S. Ono, "Evaluation of Planetary Rover Wheel Performance on Sloped Loose Soil Based on Discrete Element Method," Master's thesis, Tohoku University, 2019.

[17] P. A. Cundall and O. D. L. Strack, "A discrete numerical model for granular assemblies," *Géotechnique*, vol. 29, no. 1, pp. 47–65, 1979.

[18] R. Lichtenheldt, "A novel systematic method to estimate the contact parameters of particles in discrete element simulations of soil," in *4th International Conference on Particle-based Methods – Particles*, pp. 430–441, 2015.

[19] M. Obermayr, C. Vrettos, and P. Eberhard, "A discrete element model for cohesive soil," in *III International Conference on Particle-Based Methods*, pp. 783–794, 2013.

[20] R. Lichtenheldt, "A stable implicit time integration scheme for discrete element method and contact problems in dynamics," in *V International Conference on Particle-based Methods – Fundamentals and Applications*, 2017.

[21] R. Lichtenheldt, S. Kerler, *et al.*, "partsival - Collision-based particle and many-body Simulations on GPUs for Planetary Exploration Systems," in *The 5th Joint International Conference on Multibody System Dynamics*, 2018.

[22] R. Lichtenheldt, S. Ono, and L. Stubbig, "Large scale discrete element simulation campaigns – Simulating extraterrestrial soils in partsival," in *14th World Congress on Computational Mechanics (WCCM)*, 2021.

[23] S. Ono, R. Lichtenheldt, and K. Yoshida, "Parametric influences on the behavior of planetary regolith using DEM simulations," in *Proceedings of iSAIRAS*, 2018.

[24] S. Ono, R. Lichtenheldt, and K. Yoshida, "Soil flow analysis for planetary rovers based on particle image velocimetry and discrete element method," in *ISTVS 20th International Conference*, 2021.

[25] The MathWorks, Inc., "Bayesian Optimization Algorithm in matlab 9.7.0.1586710 (r2019b)." `https://www.mathworks.com/help/stats/bayesian-optimization-algorithm.html`. Accessed: 2021-01-07.

[26] C. K. I. Williams and C. E. Rasmussen, *Gaussian processes for machine learning*, vol. 2. MIT press Cambridge, MA, 2006.

[27] P. I. Frazier, "A Tutorial on Bayesian Optimization," *arXiv preprint:1807.02811*, 2018.